Desalination and Water Treatment
www.deswater.com
doi: 10.5004/dwt.2020.26102

200 (2020) 119–130
October

Population dynamics and metabolic alternations of AOB in activated sludge under Cu shock loads

Fan Ouyang[a,*,†], Dan Peng[a,†], Xiao Su[b]

[a]*School of Traffic and Environment, Shenzhen Institute and Information Technology, Longxiang Road 2188, Shenzhen 518172, China, emails: ouyangfanily@163.com (F. Ouyang), pengdan987@hotmail.com (D. Peng)*
[b]*School of Environmental Science and Engineering, Tianjin University, Weijin Road 92, Tianjin 300072, China, email: 13821348810@126.com (X. Su)*

Received 12 November 2019; Accepted 6 May 2020

ABSTRACT

The ammonia consumption, respiration rates ($sOUR_{NH4}$), expression of functional genes (*amoA* and *hao*) and community structures of ammonia-oxidizing bacteria (AOB) under copper (Cu) shock loads were simultaneously studied. The results showed that respiratory activities and gene transcriptional responses were sensitive to Cu toxicity. Cu inhibition and nitrite accumulation stimulation co-effected the expression of *amoA*. A Cu loading concentration at the ppm (mg L^{-1}) level produced an irreversible inhibition of the expression of *hao*. The self-repair ability of *amoA* was stronger than that of *hao* under Cu shock loadings. A principal component regression analysis model revealed that soluble Cu and intracellular Cu played important roles in the inhibitory actions of Cu shock loading on AOB. Furthermore, the linear model ($R^2 = 0.92$) adequately fitted the inhibition of soluble Cu to $sOUR_{NH4}$ while the inhibition actions of the intracellular Cu on AOB respiration conformed to a biological receptor model ($I\%_{inhibition} = 100/(1 + K_i/[M])$, $K_i = 7.4$). An uncultured *Nitrosospira* sp. exhibited stronger tolerance to Cu toxicity than *Nitrosomonas* sp. in this study. The results and their understanding lead to a deep comprehension of Cu inhibitory mechanisms on AOB in complex activated sludge systems.

Keywords: Cu shock loading; Ammonia-oxidizing bacteria (AOB); Community structure; Functional gene

1. Introduction

Chemolithoautotrophic ammonia-oxidizing bacteria (AOB) are extensively existed in activated sludge and play a central role in biological wastewater treatment processes by aerobically transforming ammonia (NH_3) to nitrite (NO_2^-–N). It is reported that AOB grows slowly and is influenced by many factors in wastewater, such as pH, temperature, alkalinity, salinity, and heavy metals [1–4].

Copper (Cu) is a typical heavy metal, which is widely used in industrial manufacturing [5]. According to statistics, the Cu concentration in wastewater ranges from 5 to 1,550 mg L^{-1} [6,7]. Large quantities of Cu flow into wastewater treatment plants (WWTPs), which increases the possibility of contamination of the influent by a high level of toxic Cu. It has been demonstrated that Cu can inhibit the activity of AOB [8,9]. Various inhibitory concentrations of Cu (ranging from 5 to 150 mg L^{-1}) on nitrification have been reported under different experimental conditions [10,11]. However, there is no unified conclusion on the threshold value of Cu inhibition on AOB. Therefore, the toxicity of Cu to AOB is of specific concern.

Previous studies estimating the inhibitory effects of Cu on AOB are mainly based on the ammonia uptake rate,

* Corresponding author.

†These authors are considered as the co-first author.

oxygen uptake rate, and biomass growth [10,12]. With the development of microbial technology, more information about cellular metabolism and the genetic reactions of AOB is now known. It has been revealed that the transformation of ammonia to nitrite by AOB involves two enzymes, ammonia monooxygenase (AMO) and hydroxylamine oxidoreductase (HAO). AMO oxidizes NH_3 to hydroxylamine (NH_2OH), and HAO further oxidizes the NH_2OH to NO_2^- [13]. Moreover, researchers have determined that *amoA* and *hao* are the main functional genes of AOB coding for AMO and HAO, respectively [14]. Furthermore, the expression of some functional genes can correlate with the activity of the enzymes thereby encoded. However, genetic responses used to estimate the inhibitory effects of Cu on AOB are only reported in a few studies.

Currently, much information on the taxonomic distribution of AOB has been obtained. All of the recognized genera of AOB so far have been limited to two phylogenetically distinct groups affiliated with the classes *Betaproteobacteria* and *Gammaproteobacteria* within the phylum *Proteobacteria* [15,16]. It has been demonstrated that toxic exposure could induce shifts in AOB community structures. Also, it has been indicated by different researchers that the majority of dominant species gradually evolved to resist the toxicity of heavy metals [17,18]. It is found that *Nitrosospira* sp. abruptly replaced *Nitrosomonas* sp. and *Nitrosococcus* sp. to become the predominant groups as a result of cadmium (Cd) shock loading [19]. Another study reported that after 8 weeks of exposure to less than 150 mg L^{-1} of nickel (Ni), the *Nitrosomonas oligotropha* lineage demonstrated a stronger tolerance than the *Nitrosomonas*-like cluster, while after 6 weeks of 150 mg L^{-1} of Ni exposure, *Nitrosospira* became the dominant AOB group. We have discovered that *Nitrosomonas* sp. was the predominant AOB in activated sludge systems with long term intermittent Cu exposures when the Cu loading increased from 5.5 to 28.2 mg L^{-1} [20]. However, this result only reflected the long term effects of Cu to AOB community structures. Accidents of heavy metal pollution have occurred frequently in China [21], which brings high pressure to the operation of WWTPs with biological treatment processes. Therefore, the investigation on how the AOB community structure responds to Cu shock loading in a short time will help researchers to deeper understand the toxic mechanisms of Cu on AOB and provide theoretical support for solving practical engineering problems. Unfortunately, to the best of our knowledge, the community structure changes of AOB resulting from Cu shock loadings in activated sludge are seldom reported.

Scientists have discovered that the form of Cu distribution in activated sludge is one of the factors primarily responsible for the inhibition of nitrification [12,22]. However, there is still no consistent conclusion as to which Cu distribution form is the main inhibitory factor. Hu et al. [23] reported that Cu could be rapidly adsorbed by activated sludge and that the sorbed Cu concentration was not a good predictor of the inhibition of ammonia consumption. Lee et al. [24] demonstrated that aqueous $Cu(NH_3)_4^{2+}$ positively correlated with the percent inhibition of ammonia oxidation.

In this study, the toxicity impact of Cu shock loading on AOB metabolic activities, including the ammonia consumption efficiency, the specific oxygen uptake rates for ammonia oxidation ($sOUR_{NH4}$) was separately detected. Real-time reverse transcription-polymerase chain reaction (real-time RT-PCR) was employed to quantify the expression of the *amoA* and *hao* genes of AOB. The community shifts of AOB were investigated by denatured gradient gel electrophoresis (DGGE). For further understanding of the Cu toxicity mechanism on AOB, a model is built to investigate the correlation among the forms of Cu distribution and the respiration rates of AOB.

2. Materials and methods

2.1. Activated sludge cultivation and reagents

Activated sludge was cultivated in five identical sequencing batch reactors (SBRs) with effective volumes of 5 L each. The sketch of one SBR is shown in Fig. 1. A timing controller was applied to operate the SBR system automatically. The temperature was kept at 25°C ± 1°C. The dissolved oxygen (DO) in the aerobic steps was kept above 2.0 mg L^{-1}.

The inoculated sludge was obtained from a local industrial WWTPs. Reactors were fed an inorganic medium devoid of organic carbon, with ammonium (75 mg of N/L, NH_4Cl) as the sole energy source. Micronutrients were added by dissolving the following chemicals in ultrapure water (mg L^{-1}): KH_2PO_4 (30), $MgSO_4{\cdot}7H_2O$ (20), $FeSO_4{\cdot}7H_2O$ (2.5), $ZnSO_4{\cdot}7H_2O$ (0.25), $CaCl_2{\cdot}2H_2O$ (10), $CoCl_2{\cdot}6H_2O$ (0.05 μg L^{-1}), and MoO_3 (1.50 μg L^{-1}). To maintain the pH at 7.8 ± 0.1 and fulfill both the carbon and alkalinity requirements in the reactor, $NaHCO_3$ (580 mg L^{-1}) was automatically added. A Cu stock solution of 50 g L^{-1} was prepared by dissolving $CuCl_2$ in an acidic solution (containing 0.37 mg L^{-1} HCl) to stabilize Cu ions in solution.

2.2. Experimental set-up

Five identical SBRs were employed simultaneously throughout the experiment and were numbered SBR-1, SBR-2, SBR-3, SBR-4, and SBR-5, respectively. The operational cycles of the five SBRs processes were similar. The running time of each cycle was 12 h which included 5 time-oriented periodic steps: wastewater filling (5 min), aeration (600 min), settling (90 min), supernatant withdrawal (5 min), and idle (20 min). 2.5 L supernatant wastewater was removed in each cycle. The collected sludge was inoculated into the five SBRs. The excess sludge was discharged periodically to keep the biomass concentration mixed-liquor suspended solids (MLSS) stable at approximately 4,500 mg L^{-1}, and consequently, a hydraulic residence time of 10 d was achieved in each reactor. SBR-1 was used as a control system that was filled with synthetic wastewater without Cu throughout the experiments. For the other four reactors, the SBRs were operated in three phases, including phase I (the incubation phase; cycles 1–6), in which synthetic wastewater without Cu was used to fill the four SBRs, and the NH_4^+–N concentration in the effluent from each SBR was maintained lower than 0.5 mg L^{-1}; phase II (the Cu shock-loading phase; cycle 7), in which synthetic wastewater with Cu stock solution addition was provided for SBR-2, SBR-3, SBR-4, and SBR-5 to make the Cu

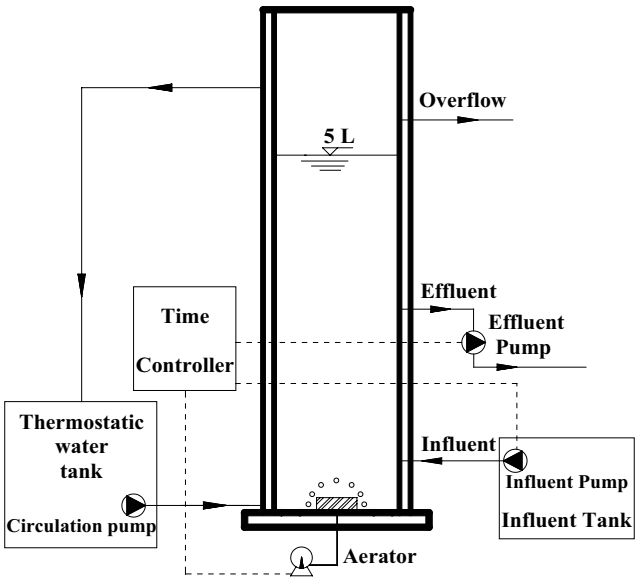

Fig. 1. Schematic of the SBR system.

concentration in the SBR reached 30, 50, 90, and 150 mg L^{-1}, respectively; and phase III (recovery phase; cycles 8–17), in which synthetic wastewater without Cu was provided for the four reactors again to explore the recovery capabilities of the activated sludge systems. At the end of the aeration periods in cycle 6, cycle 7, and cycle 16, a certain amount of activated sludge was taken out from the five SBRs for analyses of $sOUR_{NH4}$, DGGE, and real-time RT-PCR. Aliquots of sludge were taken out from the five SBRs at the end of the aeration periods in cycle 6–16 for Cu distribution analysis.

2.3. sOUR assay

The sOUR is defined as the oxygen consumption per minute per g sludge and is expressed as a specific oxygen consumption rate in mgO_2 g^{-1} MLSS min^{-1}. The $sOUR_{NH4}$ was measured by a respirometer according to a determination method reported in a previous study [25]. Briefly, assays were performed at a completely closed water-jacketed glass vessel (volume = 100 mL). Temperature and pH in the vessel were the same as in the SBR. Sludge aliquots (50 mL) were collected from the SBR, saturated with pure oxygen, and transferred to the vessel. This vessel was carefully closed. DO concentrations in the vessel were measured with a DO probe (REX model JPBJ-608, China). Sludge samples were mixed during measurement by means of magnetic stirrer at 150 rpm. First, after the DO concentration had decreased with about 3 mg L^{-1}, $NaClO_3$ was added to the mixed liquor sample (final concentration is 2.13 g L^{-1} $NaClO_3$) and OUR was determined. Then, after the DO had decreased with another 2 mg L^{-1}, allylthiourea (ATU) was added to the mixed liquor sample (final concentration was 5 mg L^{-1}) and remained OUR was measured. The difference between the OUR with $NaClO_3$ and with both $NaClO_3$ and ATU represented the oxygen uptake due to NH_4^+–N oxidation. Finally, the sludge aliquots were removed from the vessel for MLSS determination. Duplicate samples were measured each time.

The calculation equation of the inhibition rate of sOUR is as follows:

$$\text{Inhibition rate}\ (\%) = \frac{\left(\text{sOUR}_{\text{control}} - \text{sOUR}_{\text{Cu}}\right)}{\text{sOUR}_{\text{control}}} \times 100\% \quad (1)$$

where $sOUR_{control}$ was measured in cycle 6, and $sOUR_{Cu}$ was measured in cycle 7 or cycle 16 for each SBR.

2.4. DNA/RNA extraction and real time RT-PCR analysis

A Soil DNA Kit E.Z.N.A.® (OMEGA D5625-01, USA) and an RNeasy Plus Mini Kit (Qiagen, Germany) was used to isolating the total DNA and RNA according to the manufacturer's instructions, respectively. A reverse transcriptase kit (Promega, USA) was used to perform reverse transcription of the RNA to cDNA. Real-time PCRs (qPCR) was performed to detect the transcriptional responses of *amoA* and *hao* for each sample. Table 1 lists the primers of *amoA*, *hao* and 16S rRNA (16S ribosomal RNA) used in this study. Triplicate sets of cDNA were dyed by using SYBR Green I double-stranded DNA binding dye (Takara, Japan).

2.4.1. qPCR analysis

The real-time PCR analyses were performed on a Bio-Rad iQ5 instrument to quantify bacteria genes (*amoA*, *hao*, and 16S rRNA). The reactions were performed in a final volume of 25 mL of the reaction mixture (SYBR Green I double-stranded DNA binding dye, Takara) including 0.25 mM of each primer and 1 mL of cDNA. The PCR procedure for *amoA*, *hao*, and 16S rRNA genes started with an initial DNA denaturation (94°C for 5 min), followed by 40 cycles of 30 s at 94°C (denaturing), 30 s of annealing at the temperatures specified in Table 1, and 1 min at 72°C (extension), followed by a final extension of 10 min at 72°C. At the end of the reaction, association curves of the products were generated with temperature ramping from 65°C to 95°C (0.5°C per reading, 30 s hold).

2.4.2. Preparation for standard curves in the qPCR analysis

Standard curves were established before qPCR analyses on a Bio-Rad iQ5 instrument (Bio-Rad Company, CA, USA) to quantify *amoA*, *hao*, and 16S rRNA genes. Normal PCR amplification assays were conducted in a Biometra T100 gradient thermal cycler (Biometra). The PCR mixture (25 μL) contained 1 μL diluted DNA extract of activated sludge sample from SBR-1 at cycle 6 as the template, 1.5 μmol L^{-1} of each primer, 2 μL 250 μmol L^{-1} of each deoxyribonucleoside triphosphate (dNTP), 1.25 U Taq DNA polymerase (Takara), and 2.5 μL of 10xPCR buffer (Takara). For each DNA extract, triplicate PCR tubes were analyzed for the presence of each target gene. A negative control, consisting of the reaction mixture without DNA, was used in each PCR run. The PCR procedures for *amoA*, *hao*, and 16S rRNA genes were identified with the qPCR. The size and specificity (unique band) of PCR products were determined by comparison with DNA standards (Marker I, TransGen) after 1.5% (w/v) agarose gel electrophoresis. Fresh PCR

Table 1
PCR primers and PCR conditions

Gene	Target	Nucleotide sequence	Annealing temperature (°C)	Amplicon size (bp)	Reference
amoA-F	*amoA*	5′-GGGGTTTCTACTGGTGGT-3′	55.0	491	[27]
amoA-R		5′-CCCCTCKGSAAAGCCTTCTTC-3′			
hao-F	*hao*	5′-AAYCTKCGCTCRATGGG-3′	50.0	738	[28]
hao-R		5′-GGTTGGTYTTCTGKCCGG-3′			
16S-F	16S rRNA	5′-CGGTGAATACGTTCYCGG-3′	57.5	126	[29]
16S-R		5′-GGWTACCTTGTTACGACTT-3′			
CTO189fA/B(C)	AOB	5′-CCGCCGCGCGGCGGGCGGGGCGGGGGCACGG-GGGGAGRAAAGCAGGGGATCG-3′	57.0	465	[30]
–CTO654		5′-CGCCCGCCGCGCGGCGGGCGGGGCGGGGG-CACGGGGGGAGGAAAGTAGGGGATCG-3′			
F357-GC	16S rRNA	5′-CGCCCGCCGCGCGCGGCGGGCGGGGCGGGGG-CACGGGGGGCCTACGGGAGGCAGCAG-3′	55.0	169	[31]
R518		5′-CCTACGGGAGGCAGCAG-3′			

products of *amoA*, *hao* and 16S rRNA genes were recovered, purified, ligated onto pGEM-T easy vector (Promega, USA), and transformed into *Escherichia coli* DH5α according to the manufacturer's instructions (TransGen, China). Positive clones were screened by the blue-white selection, and PCR and sequencing were used to verify the cloning of the target genes. Plasmids carrying target genes were chosen as the standards for qPCR. Plasmids carrying target genes were extracted using a plasmid extraction kit (Takara, Japan). The concentration and quality of the plasmid were determined by spectrophotometry analysis and agarose gel electrophoresis. The copy number of each target gene per microliter of the plasmid solution was calculated as previously described [26]. Eight-point standard curves for qPCR were generated using 10-fold serial dilutions of the plasmid carrying target genes. R^2 values were higher than 0.996 for all standard curves. According to the standard curves, the Ct value of each sample was used to calculate the gene copy numbers of *amoA*, *hao* and 16S rRNA genes.

2.5. Denatured gradient gel electrophoresis

2.5.1. Nested PCR

The nested PCR technique was performed to amplify the specific 16S rRNA segments of AOB for DGGE analysis. In the primary reaction, a specific primer was employed to collect DNA fragments. Then, in the secondary reaction, the products of the primary reaction were amplified with universal primers. Details of the primers can be found in Table 1. The amplified products from the second PCR were confirmed by 1.5% (wt./vol.) agarose gel electrophoresis at 0.5% TBE buffer with gold view stain.

2.5.2. DGGE analysis

DGGE, referred to a previous study, was detected by the DGGE-2001 System (C.B.S. Scientific, USA). PCR products of the second reaction were separated in an 8% (w/v) polyacrylamide denaturing gradient gel in 1 × TAE. The denaturing gradients of the polyacrylamide gels ranged from 35 to 55% (where 100% denaturant consists of 7 M urea and 40% formamide in deionized water). Electrophoresis was carried out at 60°C and 150 V in 1 × TAE buffer for 6 h. The gels were then stained using ethidium bromide solution for 15 min. A gel imager (Gel Doc XR+, Bio-Rad, USA) was used to photograph the gel. QuantityOne (version 4.62, Bio-Rad, USA) was employed to analyze the gel images. Selected DNA bands in the gels were excised and eluted for sequencing. The details of the elution process can be found in previous studies [32]. Each selected band was sent to Shanghai Majorbio Bio-pharm Technology Co., Ltd., (China) for sequencing.

2.6. Cu distribution detection in an activated sludge system

To investigate the toxic effects of Cu on AOB, the forms of Cu distribution in the activated sludge system were detected. Cu was grouped into three existing forms: soluble Cu, elutable Cu and non-elutable Cu. The Cu concentration was measured according to the standard acid digestion method [33] by flame atomic absorption spectroscopy (Model WFX-130, Beijing Rui-Li Co., China). For the total Cu concentration, 10 mL of activated sludge solution was collected and directly digested. Another 10 mL of activated sludge solution was collected and filtered through a 0.45 μm membrane. The Cu concentration in the supernatant was directly measured as soluble Cu. Sludge left on the membrane was treated by a modified ethylenediaminetetraacetic acid (EDTA) washing procedure [34]. Briefly, the left activated sludge was re-suspended in 10 mL of washing solution (1 mmol L^{-1} EDTA, pH 7.0, and 0.1 mol L^{-1} NaCl), vibrated at 150 rpm for 30 min and centrifuged at 1,600 g for 5 min. Then, the supernatant was removed. The procedures of washing, centrifugation, and supernatant removal were done twice. Finally, the washed sludge was digested for the measurement of non-elutable Cu. The elutable Cu concentration was calculated by

deducting the soluble Cu and non-elutable Cu from the total Cu concentration. Duplicate samples were measured each time.

2.7. Principle component regression models

The relationships between $sOUR_{NH4}$ and the three forms of Cu (i.e., soluble Cu, elutable Cu, and non-elutable Cu) at cycle 7 were analyzed through a principal component regression analysis [35] using the following model:

$$Y = A_0 + A_1X_1 + A_2X_2 + A_3X_3 \quad (2)$$

where Y is the value of sOUR; X_1, X_2, and X_3 are the concentrations of soluble Cu, elutable Cu, and non-elutable Cu, respectively; A_0, A_1, A_2, and A_3 is the affinity coefficients. The higher the absolute values of the affinity coefficients, the greater were the contribution of the variables (soluble Cu, non-elutable Cu, and elutable Cu) to Y.

2.8. Other analytical methods

Homogenized sludge aliquots (10 mL) at the end of the aeration periods in each cycle were collected from the five SBRs for the analysis of the concentrations of MLSS and mixed-liquor volatile suspended solids (MLVSS) by using the methodology described in Standard Methods 2540 [33]. 100 mL of the effluent in each cycle from the five SBRs were collected and vacuum filtered through a 0.45 μm filter membrane for the measurements of NH_4^+–N and NO_2^-–N concentration. The measurement methods were described in Standard Methods 4500-NH_3 and 4500-NO_2^- respectively [33].

The removal efficiency of NH_4^+–N in the reactor was calculated using Eq. (3):

$$I_{NH3} - \text{renmonve}\% = \left(1 - \frac{C_{NH3}}{C_{NH3\text{-influent}}}\right) \times 100\% \quad (3)$$

where I_{NH3}-renmonve% represents the value of NH_4^+–N remove efficiency, $C_{NH3\text{-effluent}}$ and $C_{NH3\text{-influent}}$ represents the concentration of NH_4^+–N in the effluent and influent of the SBR, respectively.

3. Results and discussion

3.1. Influence of Cu shock loading on the substrate metabolic activity of AOB

As shown in Fig. 2a, SBR-1, as a control, presented an efficient and sustainable NH_4^+–N consumption of 99.7%. This suggested that AOB exhibited pronounced biological activity. In SBR 2-5, with Cu shock loadings of 30, 50, 90 and 150 mg L^{-1}, respectively, the concentrations of NH_4^+–N in the effluent were rapidly increased. Higher dosages of Cu caused greater decrements of NH_4^+–N removal efficiencies from cycle 8 to 17. The NH_4^+–N removal efficiencies further declined in SBR 2-5 after the termination of the Cu addition and then increased. In SBR-2 and SBR-3, the NH_4^+–N removal efficiencies recovered to 97.3%, and 93.2% in cycle 13,

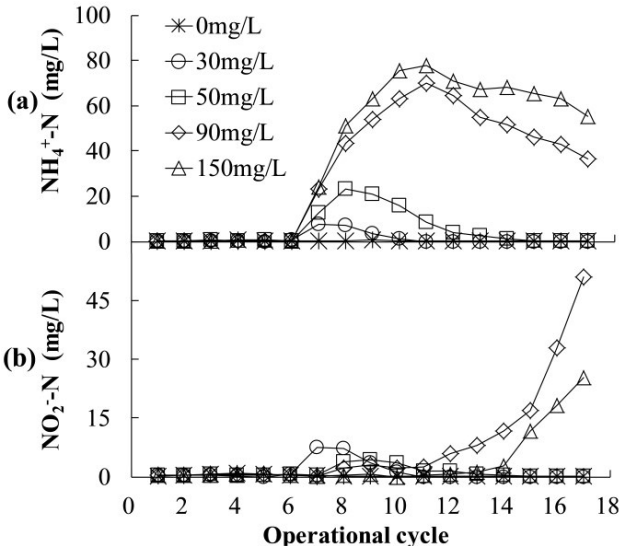

Fig. 2. Effects of Cu shock loadings on the concentrations of NH_4^+–N and NO_2^-–N.

whereas the NH_4^+–N removal efficiencies in SBR-4 and SBR-5 only increased to 51.1%, and 26.3% at the end of the experiment. This indicated that higher shock loadings of Cu (90 and 150 mg L^{-1}) severely inhibited the NH_4^+–N consumption-ability of AOB and the recovery of the NH_4^+–N consumption-ability of AOB was a rather slow and difficult process.

The NO_2^-–N accumulation was observed (Fig. 2b). Small, short-term rises in NO_2^-–N accumulations in the effluent appeared in SBR-2 and SBR-3 with Cu shock loadings of 30 and 50 mg L^{-1}, respectively. While in SBR-4 and SBR-5 with Cu shock loadings of 90 and 150 mg L^{-1}, respectively, the NO_2^-–N accumulation were gradually increased after the termination of the Cu addition. In SBR processes, AOB and nitrite-oxidizing bacteria (NOB) coexist in the activated sludge system. AOB oxidizes NH_4^+–N to NO_2^-–N; NOB then oxidizes NO_2^-–N to nitrate (NO_3^-–N). Researchers have demonstrated that NO_2^-–N accumulation is based on the inhibition of NOB [36]. Therefore, NO_2^-–N accumulation in the present paper may attribute to the Cu inhibition on NOB activity. Furthermore, a previous study has shown that 6.6 mg L^{-1} of NO_2^-–N can inhibit 90% ammonia oxidation activity of AOB in enrichment culture [37]. Pure culture tests were employed to explore the inhibitory mechanism and showed that NO_2^-–N specifically and irreversibly inactivate AMO of *Nitrosomonas europaea* [38,39]. Thus, it is likely that NO_2^-–N accumulation partly contributes to the inhibitions of ammonia consumption in the present paper. Meanwhile, various reports about Cu toxic effects on AOB pure cultures have been published [40]. Accordingly, further research on the separate contributions of Cu and NO_2^-–N toxicity to the activity of AOB in the activated sludge system is needed.

3.2. Influence of Cu shock loadings on the respiration activity of AOB

Actually, the substrate removal efficiency is only the external performance of the system, and the respiration rate

can better reflect the metabolic level of the microorganism itself. As shown in Fig. 3a, the $sOUR_{NH4}$, which characterized the respiration rates of AOB, was more subject to Cu toxicity than the NH_4^+–N consumption efficiency. With the loadings of 30, 50, 90 and 150 mg L^{-1} Cu, the inhibition ratios for $sOUR_{NH4}$ were 41.3%, 60.3%, 72.4% and 84.9% at cycle 7, respectively. During the recovery phase, each reactor showed a certain ability to recover. The respiration activity of AOB in SBR-2 and SBR-3 was naturally recoverable at the end of the recovery phase, while in SBR-4 and SBR-5, the inhibition rates of $sOUR_{NH4}$ were still 57.0% and 75.7%, respectively.

As discussed in part 3.1, the NH_4^+–N consumption activity of AOB could be inhibited by NO_2^-–N accumulation. Whereas, the literature focused on NO_2^-–N toxicity to the respiratory activity of AOB is limited. Contreras et al. [41] reported that NO_2^-–N toxicity to AOB respiration conformed to a competitive inhibition model. The inhibitory mechanism was that N_2O_4 could be formed abiotically from NO_2^-–N and competed for the same enzymatic site of AMO with O_2. At cycle 7, the inhibition rates of $sOUR_{NH4}$ in each SBR reached the maximum value, yet NO_2^-–N accumulation did not be observed. Thus, the main reason for the $sOUR_{NH4}$ inhibition might be the toxic effect of Cu. At cycle 16, the inhibition rates of $sOUR_{NH4}$ in SBR 2-5 decreased to 22.8%, 29.5%, 57.0%, and 75.7%, respectively. Meanwhile, the concentration of NO_2^-–N in SBR 2-5 was 0.009, 0.125, 50.875, and 25.27 mg L^{-1}, respectively. It can be inferred that the inhibition of $sOUR_{NH4}$ at cycle 16 was probably caused by the co-effects of Cu and NO_2^-–N.

3.3. Cu distribution in the SBR

The adsorption processes of Cu in activated sludge with Cu shock loading of 30, 50, 90, and 150 mg L^{-1} present a similar trend (Figs. 4a–d). As shown in Fig. 4a, in the Cu loading cycle (cycle 7), the Cu shock loads dramatically distributed as soluble Cu, elutable Cu and non-elutable Cu. The quantities of the elutable and non-elutable Cu accounted for 99% of the total Cu, which suggested that most of the Cu was adsorbed by the activated sludge. The concentrations of the elutable Cu reached their maximum in cycle 7, while they were sharply decreased in the subsequent recovery cycles (cycles 8–12). Meanwhile, the concentrations of the non-elutable Cu slowly increased and reached a plateau in cycles 8–12. It has been revealed that the elutable and non-elutable Cu approximately corresponded to extracellular and intracellular Cu, respectively [23]. Metal portioning (uptake) including extracellular sorption, transmembrane transport, and intracellular accumulation in many microorganisms [42]. When metals are present in excess, they can across the bacterial cell membrane and accumulate in the cell by fast and relatively nonspecific metal transport systems [23,43]. Thus, it could be inferred that there was transport of Cu from elutable Cu to non-elutable Cu, which contributed to the decrease in the elutable Cu in cycles 8–12. Moreover, the influent might have a flushing function on the elutable Cu to transform it into soluble Cu. The alternation of influent filling and effluent withdrawal further resulted in the drop in soluble Cu. In cycle 13–15, the concentration variation curves of the three Cu distribution forms flattened out. It could be speculated that a relative equilibrium of Cu distribution in the SBRs might have been obtained during this period. The concentration of Cu in SBR-2, SBR-3, SBR-4, and SBR-5 was 4.48, 4.92, 7.83, and 14.55 mg Cu g^{-1} MLVSS, respectively. The remaining percentage of Cu in SBR-2, SBR-3, SBR-4, and SBR-5 was 50.5%, 34.1%, 33.3%, and 35.0% by comparison with their initial Cu loading concentrations.

According to the principal component regression models, the following equations were obtained:

$$Y_1 = 0.095 - 0.015X_1 - 0.140\times10^{-3}X_2 - 0.117\times 10^{-2}X_3 \left(R^2 = 0.98,\ p = 0.005\right) \quad (4)$$

The negative affinity coefficients in Eq. (4) indicate that $sOUR_{NH4}$ is negatively correlated with the concentrations of the three forms of Cu. There is no general consensus on

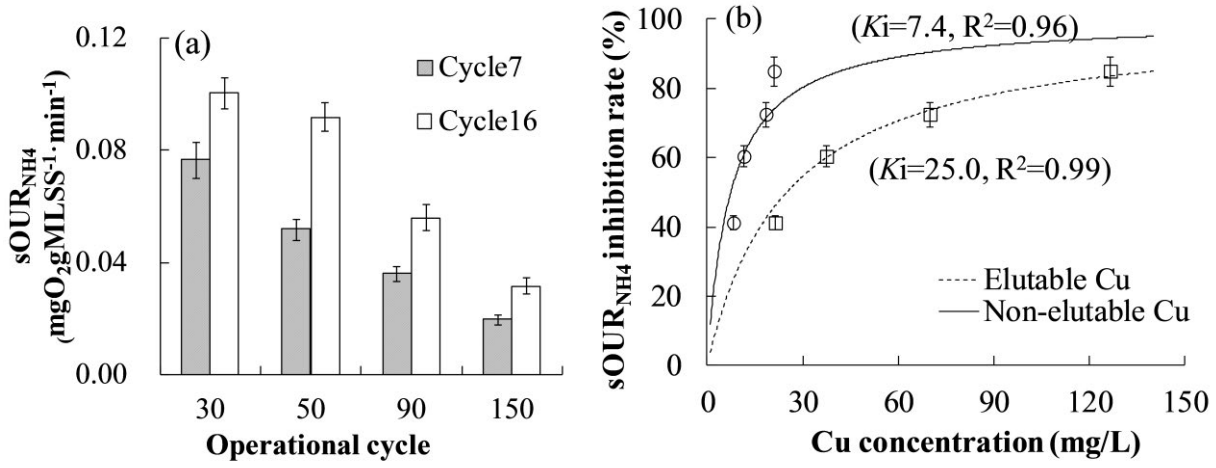

Fig. 3. (a) Values of $sOUR_{NH4}$ at the end of each Cu loading and recovery period and (b) $sOUR_{NH4}$ inhibition rates as a function of intracellular and extracellular Cu concentrations, respectively.

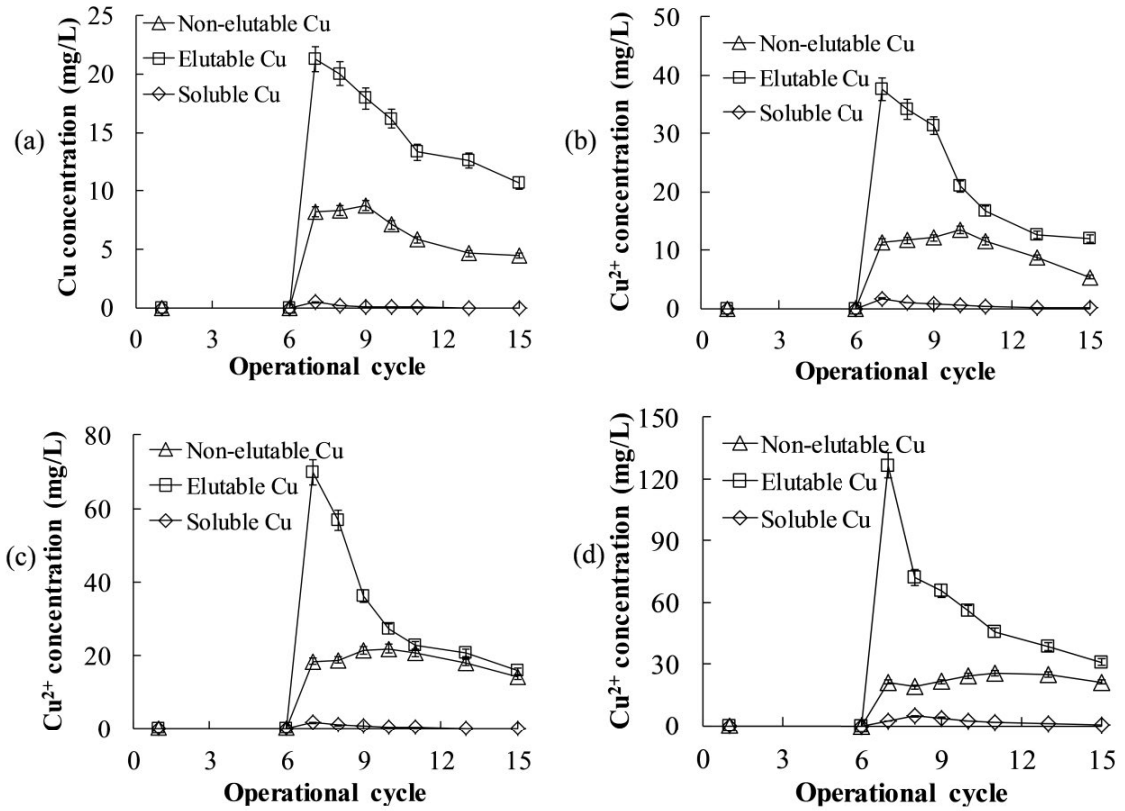

Fig. 4. Cu distributions in the activated sludge solution dosed with (a) 30 mg L^{-1}, (b) 50 mg L^{-1}, (c) 90 mg L^{-1}, and (d) 150 mg L^{-1} of Cu.

which one is the main factor causing the toxic inhibition among the three forms of Cu. Based on comparing the absolute values of the affinity coefficients, the toxicity of the three Cu distributions to $sOUR_{NH4}$ was in the order of soluble Cu > non-elutable Cu > elutable Cu. Free metal cations are generally thought to be the most toxic metal species [44]. This point was supported by our results. Soluble Cu in the present paper was the most toxic Cu distribution form to AOB respiration. The toxicity mechanism of the non-elutable Cu might be partly attributed to the interaction of the intracellular Cu ions with proteins which impairs protein folding and promotes aggregation [45]. Furthermore, intracellular reactive oxygen species induced by Cu^{2+} may cause lipid peroxidation, cellular metabolic malfunction, and cell membrane disruption [46–49] and was probably another reason for intracellular Cu toxicity to AOB respiration. The elutable Cu showed the weakest link with the $sOUR_{NH4}$. Studies have determined that extracellular polymeric substances (EPSs) in activated sludge from a barrier to relieve the toxicity of the extracellular Cu [50,51]. The proteins and humic substances are strong ligands for Cu^{2+} to defuse Cu toxicity to microorganisms [51]. Therefore, the toxicity of the elutable Cu could be relieved by the EPSs.

3.4. $sOUR_{NH4}$ inhibition by Cu

An empirical biological receptor model [23], as shown in Eq. (5), was employed to investigate the correlations of inhibition rates of $sOUR_{NH4}$ with the three Cu forms.

$$I\%_{\text{inhibition}} = \frac{100}{\left(1 + K_i / [M]\right)} \tag{5}$$

where $I\%_{\text{inhibition}}$ is the sOUR inhibition rate; $[M]$ is the Cu loading concentration, (mg L^{-1}); and K_i is a half-maximum response coefficient (mg L^{-1}), representing the Cu concentration causing 50% inhibition.

The fitting results of the biological receptor model to $sOUR_{NH4}$ and Cu are shown in Table 2. The non-elutable Cu and the elutable Cu fitted well with the model (R^2 = 0.96 for $sOUR_{NH4}$-non-elutable Cu, R^2 = 0.99 for $sOUR_{NH4}$-elutable Cu). This result was also consistent with one of our previous studies in which nitrifying bacteria were inhibited by long-term Cu gradient loadings [52]. The soluble Cu present poor correlation with $sOUR_{NH4}$ (R^2 = 0.83) (Table 2), which suggested that soluble

Table 2
Results of the biological receptor model to $sOUR_{NH4}$ and Cu

	K_i	R^2
$sOUR_{NH4}$- non-elutable Cu	7.4	0.96
$sOUR_{NH4}$-elutable Cu	25.0	0.99
$sOUR_{NH4}$-soluble Cu	0.72	0.83

K_i is the half-maximum response coefficient (mg L^{-1}), which represents the Cu concentration that causes 50% inhibition.

Cu inhibition to $sOUR_{NH4}$ could not be described by the empirical biological receptor model. A simple linear model adequately fit the inhibition of soluble Cu to $sOUR_{NH4}$ (R^2 = 0.92 vs. 0.83). The soluble Cu concentration causing 50% inhibition was estimated at 0.96 mg L^{-1}.

3.5. Influence of Cu shock loads on amoA and hao expression

Studies have confirmed that the normalized gene expression is directly proportional to the amount of RNA of a certain target sequence (i.e., the target gene) relative to the amount of RNA of the reference gene [53]. The relative abundances of the *amoA* and *hao* genes to per 16S rRNA are given in Fig. 5 to describe the variations of the *amoA* and *hao* gene expressions respectively. As shown in Fig. 5, the concentration of Cu had a significant effect on the gene expression of the *amoA* and *hao* gene (analysis of variance; $p < 0.05$). The relative gene expression levels of the *amoA* genes in all samples in the Cu loading phases were less than those of the control, which suggested that Cu concentration above 30 mg L^{-1} would inhibit the expression of *amoA*. In contrast, the variations of the *amoA* gene relative expression levels in the recovery period seemed to become irregular. The relative expression level of *amoA* in the recovery phase was higher than that of the Cu shock loading phase when the Cu shock loading concentration was 30 mg L^{-1}, which suggested that 30 mg L^{-1} of Cu inhibition on the expression of *amoA* was recoverable. However, for the 50 mg L^{-1} of Cu shock loading, the relative expression level of *amoA* in the recovery period was lower than that in the control, which indicated that the toxic effect of 50 mg L^{-1} of Cu on the expression of *amoA* was irreversible. The relative expression level of *amoA* in the recovery phase was higher than that of the control when the Cu shock loading concentration was 90 mg L^{-1}. Meanwhile, NO_2^-–N accumulation reached the maximum value in the effluent (Fig. 2). Literature has reported that a gradual increase in *amoA* transcripts level coincided with an increase in NO_2^-–N concentration in the SBR. And the possible reason is that the expression of *amoA* was up-regulated to maintain the AMO activity under NO_2^-–N stimulation to conserve energy for cell metabolism [54]. The relative expression level of *amoA* in the recovery period was lower than that of the control when the Cu shock loading concentration was 150 mg L^{-1}. This was probably due to the combined effects of NO_2^-–N accumulation stimulation and Cu toxicity inhibition since both the concentration of Cu and NO_2^-–N was noticeably higher in this period.

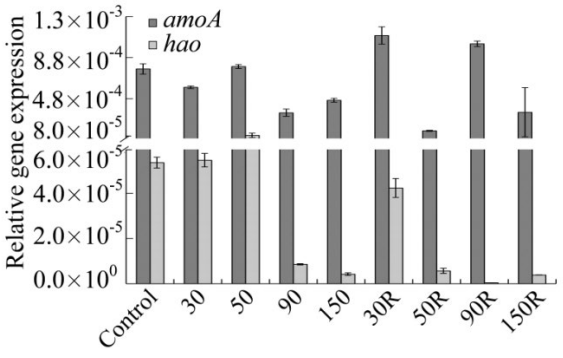

Fig. 5. Relative gene expressions of *amoA* and *hao* genes at the end of each Cu loading and recovery period, respectively.

Interestingly, the *hao* gene presented different responses to Cu exposure. The presence of Cu (30 and 50 mg L^{-1}) enhanced the expression level of the *hao* genes ($(5.45 \pm 0.30) \times 10^{-5}$ for 30 mg L^{-1} and $(1.13 \pm 0.21) \times 10^{-4}$ for 50 mg L^{-1}) vs. that of the control ($(5.35 \pm 0.24) \times 10^{-5}$). Significant decreases were observed in the relative gene expression level of *hao* on exposure to 90 and 150 mg L^{-1} of Cu. These results indicated that a relatively low level of Cu loading was exerting a significant selective pressure that facilitated the expression of *hao*. Nevertheless, when the Cu loading concentration exceeded an acceptable level, Cu could inhibit the expression of *hao*. In the recovery phases, the abundances of *hao* genes in all samples were less than those of the control, which suggested that Cu concentration at the ppm (mg L^{-1}) level would produce an irreversible inhibition to the expression of *hao*. Furthermore, it seems that *hao* is more likely to be influenced by Cu than *amoA* when under Cu shock loading conditions.

3.6. Diversity and phylogenetic changes of AOB under Cu shock loadings

The diversity and phylogenetic changes in AOB under Cu shock loads were studied by DGGE. The DGGE profiles of the PCR-amplified AOB 16S rRNA gene fragments are shown in Fig. 6. The intensity and color depth of the bands, which symbolized the abundance of the species, were greater in A1 and A2 than in those in other samples which suggested that 30 and 50 mg L^{-1} of Cu facilitated the dissemination and proliferation of the AOB population. However, the intensity of the bands in A5–A8 (recovery phase) were lower than the corresponding Cu-fed samples. It is indicated that Cu could stimulate the proliferation of the AOB species in a short period, while long-term exposure to Cu would decrease the population of the AOB group.

As shown in Fig. 6, band *a* was brightened in samples A1, A2, A3 and A4 (cycle 7) but exhibited a decreasing abundance in samples A5, A6, A7 and A8 (cycle 17). The result indicated that the AOB population represented by bands *a* could out-compete other AOB species under Cu shock loadings, while they failed in the recovery phase without Cu. Bands *b* and *d* were detected in the A_0 sample, while they disappeared in A1-A8 suggesting that the Cu could cause fatal damage to them. New bands *g*, *h*, *i*, and *j* were detected in Cu-fed samples, which exhibited different responses to Cu loads. The new bands *g* and *h* were only detected in samples A1 and A2 (30 and 50 mg L^{-1} Cu-fed system), showing that they might be species suitable for proliferation in an environment containing a certain level of Cu concentration. Band *j*, which was only detected in A4, might have a stronger Cu tolerance than bands *g* and *h*. Band *k* appeared in samples A5, A6 and A8 in the recovery phase and might play an important role in the recovery of AOB activity. Noticeably, band *k* disappeared in A7, meanwhile, the nitrite accumulation concentration reached maximum value. Therefore, the disappearance of band *k* in A7 might result from the nitrite toxicity.

The major bands in the DGGE gel were excised and sequenced. All the sequencing results were submitted to the GenBank database by BLAST to search for similar sequences. The identification of these bands is shown in Table 3. More than half of the sequences exhibited homology to uncultured AOB species. To reveal the evolutionary relationships between the species listed in Table 3, a phylogenetic tree was drawn as shown in Fig. 7. It suggested that the genetic relationship among AOB species is very close. All of the AOB species were mainly affiliated with uncultured *Nitrosomonas* sp. The uncultured *Nitrosospira* sp. (i.e., band *j*), which appeared in the 150 mg L^{-1} Cu shock loading of SBR-5 in cycle 7, should have a high tolerance to the high concentration of Cu, and as a result, its abundance became richer during the competition with other AOB species. Previous studies have demonstrated that *Nitrosomonas* is one of the dominant AOB groups, and is widespread in activated sludge systems [55] and performed with high resistance to the changing circumstances. Our results are similar to this conclusion that *Nitrosomonas* is one of the more dominant AOB groups in activated sludge systems. Moreover, uncultured *Nitrosospira* sp. demonstrated a stronger Cu tolerance than uncultured *Nitrosomonas* sp. under higher Cu shock loadings in our results. Interestingly, NO_2^-–N accumulation was probably another important factor affecting the AOB community structure. The appearance of *Nitrosomonas* sp. HKU20 (i.e., band *k*) coincided with the NO_2^-–N accumulation. And when the NO_2^-–N concentration reached a maximum value of 50.85 mg L^{-1}, *Nitrosomonas* sp. was disappeared. Therefore, different environmental conditions would impact the AOB composition in activated sludge systems. Different situations should be evaluated case by case [56].

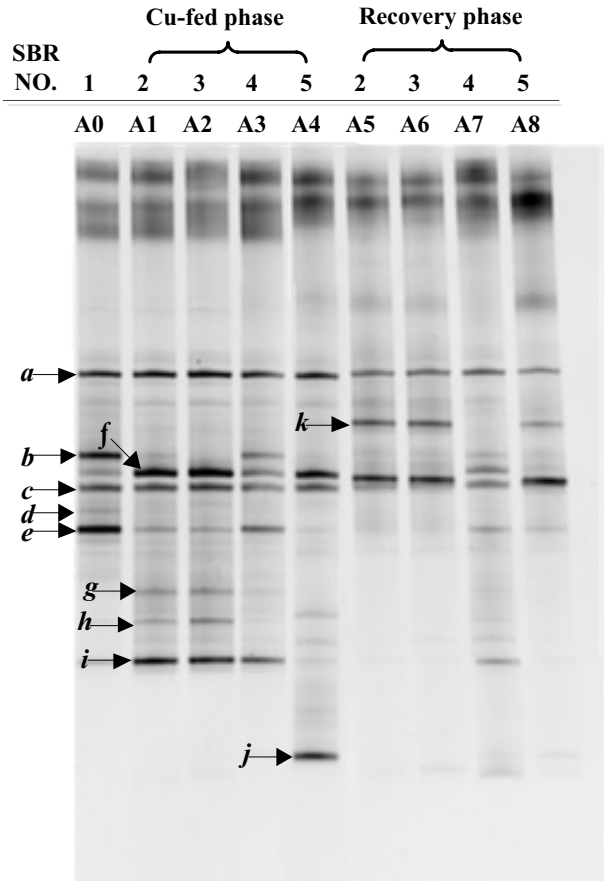

Fig. 6. The phylogenetic profile of each sample at the end of each Cu loading and recovery period detected by DGGE.

4. Conclusion

The inhibitory effects of Cu shock loading on AOB including metabolism activity and community diversity in complex activated sludge systems occurred during the Cu loading phase and remained detectable in the following recovery phase. The toxicity of the three Cu forms to AOB was mainly ascribed to soluble Cu > non-elutable Cu > elutable Cu. The activity of ammonia consumption and $sOUR_{NH4}$ of AOB in the recovery phase became stronger than that in the Cu loading phase when the Cu concentration ranged from 30 to 150 mg L^{-1}. Meanwhile, the expression of *amoA*

Table 3
Results of some partial 16S rDNA sequences using BLASTN in GenBank

Band	Accession	Most closely related sequence by BLASTN	Identity
a	AY123811	*Nitrosomonas* sp. Nm59	97%
b	JF506034	Uncultured *Nitrosomonas* sp. isolate DGGE gel band A12 16S ribosomal RNA gene, partial sequence	100%
f	JF506039	Uncultured *Nitrosomonas* sp. isolate DGGE gel band A17 16S ribosomal RNA gene, partial sequence	100%
d	KF228157	*Nitrosomonas oligotropha* sp. clone G10-0AF4B_11038 16S ribosomal RNA gene, partial sequence	97%
e	JF506026	Uncultured *Nitrosomonas* sp. isolate DGGE gel band A4 16S ribosomal RNA gene, partial sequence	100%
c	JF506029	Uncultured *Nitrosomonas* sp. isolate DGGE gel band A7 16S ribosomal RNA gene, partial sequence	100%
g	JF506024	Uncultured *Nitrosomonas* sp. isolate DGGE gel band A2 16S ribosomal RNA gene, partial sequence	100%
h	AB900133	*Nitrosomonas* sp. KYUHI-S gene for 16S ribosomal RNA, partial sequence	99%
i	GU189063	Uncultured *Nitrosomonas* sp. isolate DGGE gel band SBR-Z-12 16S ribosomal RNA gene, partial sequence	99%
j	GQ247369	Uncultured *Nitrosospira* sp. clone Cb4 16S ribosomal RNA gene, partial sequence	100%
k	KP074944	*Nitrosomonas* sp. HKU20 16S ribosomal RNA gene, partial sequence	97%

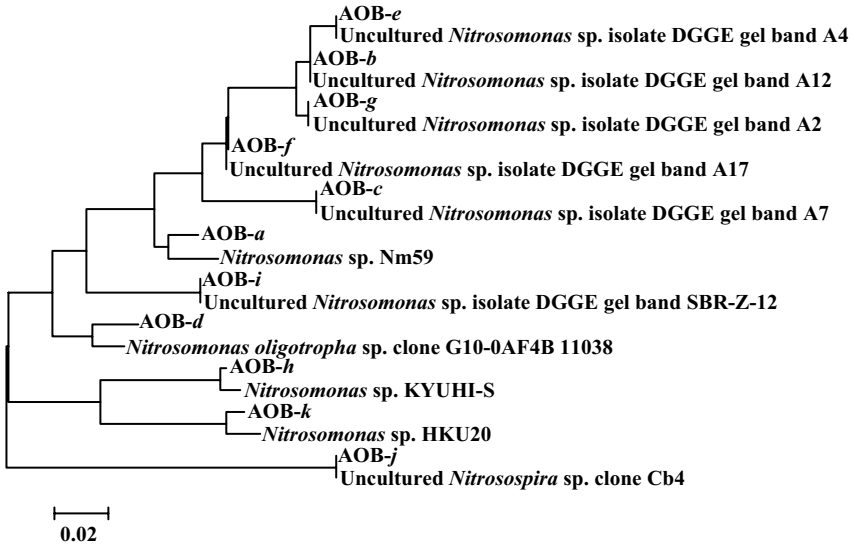

Fig. 7. Phylogenetic tree of the AOB species calculated by the neighbor-joining method.

presented different responses to Cu loadings compared to ammonia consumption and $sOUR_{NH4}$.

The Cu inhibition and NO_2^-–N accumulation stimulation co-effected the expression of *amoA*. Inhibition on the expression of *amoA* under Cu loading concentration below 30 mg L^{-1} was recoverable. Irreversible inhibition to the expression of *hao* was induced when the Cu loading concentration at the ppm (mg L^{-1}). Furthermore, *hao* demonstrated more sensitivity to Cu toxicity than *amoA*. The Cu loading concentration below 50 mg L^{-1} facilitates the dissemination and proliferation of Cu-tolerant AOB populations. Higher loadings of 90 and 150 mg L^{-1} Cu reduced the densities of predominant AOB species and slightly altered the community structure of the AOB groups. *Nitrosomonas* sp. was the most abundant AOB species, and an uncultured *Nitrosospira* sp. appeared more tolerant of Cu toxicity than *Nitrosomonas* sp. in this study.

Acknowledgments

The author would like to thank the School scientific research cultivation project of Shenzhen Institute of Information Technology (QN201708), Foundation for Distinguished Young Talents in Higher Education of Guangdong, China (2017GkQNCX066), Natural Science Foundation of Guangdong province of China (2018A030-313363), and Shenzhen Science & Technology Project (JCYJ20180307155011964).

References

[1] Y.Z. Peng, J.F. Gao, S.Y. Wang, M.H. Sui, Use of pH as fuzzy control parameter for nitrification under different alkalinity in SBR process, Water Sci. Technol., 47 (2003) 77–84.
[2] Y. Wang, H. Chen, Y.X. Liu, R.P. Ren, Y.K. Lv, Effect of temperature, salinity, heavy metals, ammonium concentration, pH and dissolved oxygen on ammonium removal by an aerobic nitrifier, RSC Adv, 5 (2015) 79988–79996.
[3] Z.Z. Zhang, Q.Q. Zhang, J.J. Xu, Z.J. Shi, Q. Guo, X.Y. Jiang, H.Z. Wang, G.H. Chen, R.C. Jin, Long-term effects of heavy metals and antibiotics on granule-based anammox process: granule property and performance evolution, Appl. Microbiol. Biotechnol., 100 (2016) 2417–2427.
[4] J. Gabarró, R. Ganigué, F. Gich, M. Ruscalleda, M.D. Balaguer, J. Colprim, Effect of temperature on AOB activity of a partial nitritation SBR treating landfill leachate with extremely high nitrogen concentration, Bioresour. Technol., 126 (2012) 283–289.
[5] Y. Wang, Y. Zhao, M. Ji, H. Zhai, Nitrification recovery behavior by bio-accelerators in copper-inhibited activated sludge system, Bioresour. Technol., 192 (2015) 748–755.
[6] R. Sierra-Alvarez, J. Hollingsworth, M.S. Zhou, Removal of copper in an integrated sulfate reducing bioreactor-crystallization reactor system, Environ. Sci. Technol., 41 (2007) 1426–1431.
[7] V. Stanković, D. Božić, M. Gorgievski, G. Bogdanović, Heavy metal ions adsorption from mine waters by sawdust, Chem. Ind. Chem. Eng. Q., 15 (2009) 251–256.
[8] A. Liu, J. Li, M. Li, X.Y. Niu, J. Wang, Toxicity assessment of binary metal mixtures (copper-zinc) to nitrification in soilless culture with the extended biotic ligand model, Arch. Environ. Contam. Toxicol., 72 (2017) 312–319.
[9] S. Aslan, O. Sozudogru, Individual and combined effects of nickel and copper on nitrification organisms, Ecol. Eng., 99 (2017) 126–133.
[10] V. Ochoa-Herrera, G. León, Q. Banihani, J.A. Field, R. Sierra-Alvarez, Toxicity of copper(II) ions to microorganisms in biological wastewater treatment systems, Sci. Total Environ., 412 (2011) 380–385.
[11] Y.W. Lee, Q. Tian, S.K. Ong, C. Sato, J. Chung, Inhibitory effects of copper on nitrifying bacteria in suspended and attached growth reactors, Water Air Soil Pollut., 203 (2009) 17–27.
[12] F. Çeçen, N. Semerci, A.G. Geyik, Inhibitory effects of Cu, Zn, Ni and Co on nitrification and relevance of speciation, J. Chem. Technol. Biotechnol, 85 (2010) 520–528.
[13] T.S. Radniecki, L. Semprini, M.E. Dolan, Expression of *merA*, *amoA* and *hao* in continuously cultured *Nitrosomonas europaea* cells exposed to zinc chloride additions, Biotechnol. Bioeng., 102 (2009) 546–553.
[14] P. Junier, V. Molina, C. Dorador, O. Hadas, O.S. Kim, T. Junier, K.P. Witzel, J.F. Imhoff, Phylogenetic and functional marker genes to study ammonia-oxidizing microorganisms (AOM) in the environment, Appl. Microbiol. Biot., 85 (2010) 425-440.
[15] E.V. Lebedeva, M. Alawi, F. Maixner, P.G. Jozsa, H. Daims, E. Spieck, Physiological and phylogenetic characterization of a novel lithoautotrophic nitrite-oxidizing bacterium, *'Candidatus nitrospira bockiana'*, Int. J. Syst. Evol. Microbiol., 58 (2008) 242.

[16] S. Ehrich, D. Behrens, E. Lebedeva, W. Ludwig, E. Bock, A new obligately chemolithoautotrophic, nitrite-oxidizing bacterium, *Nitrospira moscoviensis* sp. nov. and its phylogenetic relationship, Arch. Microbiol., 164 (1995) 16–23.
[17] J. Demanou, S. Sharma, A. Weber, B.M. Wilke, T. Njine, A. Monkiedje, J.C. Munch, M. Schloter, Shifts in microbial community functions and nitrifying communities as a result of combined application of copper and mefenoxam, FEMS Microbiol. Lett., 260 (2010) 55–62.
[18] J. Keshri, B.B. Mankazana, M.N. Momba, Profile of bacterial communities in South African mine-water samples using Illumina next-generation sequencing platform, Appl. Microbiol. Biotechnol., 99 (2015) 3233–3242.
[19] B. Mertoglu, N. Semerci, N. Guler, B. Calli, F. Cecen, A.M. Saatci, Monitoring of population shifts in an enriched nitrifying system under gradually increased cadmium loading, J. Hazard. Mater., 160 (2008) 495–501.
[20] F. Ouyang, M. Ji, H.Y. Zhai, Z. Dong, L. Ye, Dynamics of the diversity and structure of the overall and nitrifying microbial community in activated sludge along gradient copper exposures, Appl. Microbiol. Biotechnol., 100 (2016) 6881–6892.
[21] Y. Luo, Y. Liu, Q. Du, Q. Chen, Z. Cheng, The identification research of emergency treatment technology for sudden heavy metal pollution accidents in drainage basin based on D-S evidence theory, Water Sci. Technol., 80 (2019) 2392–2403.
[22] J.S. Song, M. Maeng, K. Lee, S.P. Pack, J.W. Lee, The role of extracellular polymeric substances in reducing copper inhibition to nitrification in activated sludge, Biotechnol. Bioprocess Eng., 21 (2016) 683–688.
[23] Z.Q. Hu, K. Chandran, D. Grasso, B.F. Smets, Impact of metal sorption and internalization on nitrification inhibition, Environ. Sci. Technol., 37 (2003) 728–734.
[24] Y. Lee, S. Ong, C. Sato, Effects of heavy metals on nitrifying bacteria, Water Sci. Technol., 89 (1997) 69–74.
[25] J. Surmacz-Gorska, K. Gernaey, C. Demuynck, P. Vanrolleghem, W. Verstraete, Nitrification monitoring in activated sludge by oxygen uptake rate (OUR) measurements, Water Res, 30 (1996) 1228–1236.
[26] T. Zhang, M. Zhang, X. Zhang, H.H. Fang, Tetracycline resistance genes and tetracycline resistant lactose-fermenting *Enterobacteriaceae* in activated sludge of sewage treatment plants, Environ. Sci. Technol., 43 (2009) 3455–3460.
[27] J.H. Rotthauwe, K.P. Witzel, W. Liesack, The ammonia monooxygenase structural gene *amoA* as a functional marker: molecular fine-scale analysis of natural ammonia-oxidizing populations, Appl. Environ. Microbiol., 63 (1998) 4704–4712.
[28] M.C. Schmid, A.B. Hooper, M.G. Klotz, D. Woebken, P. Lam, M.M. Kuypers, A. Pommerening-Roeser, H.J.M.O.D. Camp, M.S.M. Jetten, Environmental detection of octahaem cytochrome *c* hydroxylamine/hydrazine oxidoreductase genes of aerobic and anaerobic ammonium-oxidizing bacteria, Environ. Microbiol., 10 (2010) 3140–3149.
[29] M.T. Suzuki, L.T. Taylor, E.F. Delong, Quantitative analysis of small-subunit rRNA genes in mixed microbial populations via 5′-nuclease assays, Appl. Environ. Microbiol., 66 (2000) 4605–4614.
[30] G.A. Kowalchuk, J.R. Stephen, W.I.E.T.S.E. De Boer, J.I. Prosser, T.M. Embley, J.W. Woldendorp, Analysis of ammonia-oxidizing bacteria of the beta subdivision of the class proteobacteria in coastal sand dunes by denaturing gradient gel electrophoresis and sequencing of PCR-amplified 16S ribosomal DNA fragments, Appl. Environ. Microbiol., 63 (1997) 1489–1497.
[31] G. Muyzer, E.C. de Waal, A.G. Uitterlinden, Profiling of complex microbial populations by denaturing gradient gel electrophoresis analysis of polymerase chain reaction-amplified genes coding for 16S rRNA, Appl. Environ. Microbiol., 59 (1993) 695–700.
[32] G. Chen, J. Huang, X. Tian, Q. Chu, Y. Zhao, H. Zhao, Effects of influent loads on performance and microbial community dynamics of aerobic granular sludge treating piggery wastewater, J. Chem. Technol. Biotechnol., 93 (2017) 1443–1452.
[33] APHA, Standard Methods for the Examination of Water and Wastewater, 21st ed., American Public Health Association/ American Water Works Association/Water Environment Federation, Washington, 2005.
[34] M.T.S.D. Vasconcelos, M.F.C. Leal, Adsorption and uptake of Cu by *Emiliania huxleyi* in natural seawater, Environ. Sci. Technol., 35 (2001) 508–515.
[35] R. Liu, J. Kuang, Q. Gong, X. Hou, Principal component regression analysis with SPSS, Comput. Methods Programs Biomed., 71 (2003) 141–147.
[36] B. Ma, S. Wang, S. Cao, Y. Miao, F. Jia, R. Du, Y. Peng, Biological nitrogen removal from sewage via anammox: recent advances, Bioresour. Technol., 200 (2016) 981–990.
[37] N.C. Tan, M.J. Kampschreur, W. Wanders, W.L. van der Pol, J. van de Vossenberg, R. Kleerebezem, M.C. van Loosdrecht, M.S. Jetten, Physiological and phylogenetic study of an ammonium-oxidizing culture at high nitrite concentrations, Syst. Appl. Microbiol., 31 (2008) 114–125.
[38] L.Y. Stein, D.J. Arp, Loss of ammonia monooxygenase activity in *Nitrosomonas europaea* upon exposure to nitrite, Appl. Environ. Microbiol., 64 (1998) 4098–4102.
[39] L.S. Cua, L.Y. Stein, Effects of nitrite on ammonia-oxidizing activity and gene regulation in three ammonia-oxidizing bacteria, FEMS Microbiol. Lett., 319 (2011) 169–175.
[40] T. Radniecki, R. Ely, Transcriptional and physiological responses of *Nitrosococcus mobilis* to copper exposure, J. Environ. Eng., 137 (2011) 307–314.
[41] E.M. Contreras, F. Ruiz, N.C. Bertola, Inhibition of the Respiration Rate of Ammonia Oxidizing Bacteria by Nitrite, https://www.researchgate.net/publication/228508754, 2014.
[42] D. Chang, K. Fukushi, S. Ghosh, Stimulation of activated sludge cultures for enhanced heavy metal removal, Water Environ. Res., 67 (1995) 822–827.
[43] D.H. Nies, Microbial heavy-metal resistance, Appl. Microbiol. Biotechnol., 51 (1999) 730–750.
[44] P.G. Campbell, A. Tessier, D. Turner, Metal Speciation and Bioavailability in Aquatic Systems, IUPAC Series on Analytical and Physical Chemistry of Environmental Systems, Wiley, Chichester, 1995.
[45] C.M. Saporito-Magriñá, R.N. Musacco-Sebio, G. Andrieux, L. Kook, M.T. Orrego, M.V. Tuttolomondo, M.F. Desimone, M. Boerries, C. Borner, M.G. Repetto, Copper-induced cell death and the protective role of glutathione: the implication of impaired protein folding rather than oxidative stress, Metallomics, 10 (2018) 1743–1754.
[46] T. Ajiboye, M. Aliyu, I. Isiaka, F. Haliru, O. Ibitoye, J. Uwazie, H. Muritala, S. Bello, I. Yusuf, A. Mohammed, Contribution of reactive oxygen species to (+)-catechin-mediated bacterial lethality, Chem. Biol. Interact., 258 (2016) 276–287.
[47] B. Das, S.K. Dash, D. Mandal, T. Ghosh, S. Chattopadhyay, S. Tripathy, S. Das, S.K. Dey, D. Das, S. Roy, Green synthesized silver nanoparticles destroy multidrug resistant bacteria via reactive oxygen species mediated membrane damage, Arabian J. Chem., 10 (2017) 862–876.
[48] J. Lawrence, G. Swerhone, J. Dynes, A. Hitchcock, D. Korber, Complex organic corona formation on carbon nanotubes reduces microbial toxicity by suppressing reactive oxygen species production, Environ. Sci. Nano, 3 (2016) 181–189.
[49] C. Gunawan, W.Y. Teoh, C.P. Marquis, R. Amal, Cytotoxic origin of copper (II) oxide nanoparticles: comparative studies with micron-sized particles, leachate, and metal salts, ACS nano, 5 (2011) 7214–7225.
[50] J. Li, X. Liu, Y. Liu, J. Ramsay, C. Yao, R. Dai, The effect of continuous exposure of copper on the properties and extracellular polymeric substances (EPS) of bulking activated sludge, Environ. Sci. Pollut. Res., 18 (2011) 1567–1573.
[51] Y. Wang, J. Qin, S. Zhou, X. Lin, L. Ye, C. Song, Y. Yan, Identification of the function of extracellular polymeric substances (EPS) in denitrifying phosphorus removal sludge in the presence of copper ion, Water Res., 73 (2015) 252–264.
[52] F. Ouyang, H.Y. Zhai, M. Ji, H.Y. Zhang, Z. Dong, Physiological and transcriptional responses of nitrifying bacteria exposed

to copper in activated sludge, J. Hazard. Mater., 301 (2016) 172–178.
[53] P. Muller, H. Janovjak, A. Miserez, Z. Dobbie, Processing of gene expression data generated by quantitative real-time RT PCR, Biotechniques, 33 (2002) 514–514.
[54] A. Cydzik-Kwiatkowska, S. Ciesielski, I. Wojnowska-Baryła, Bacterial *amoA* and 16S rRNA genes expression in activated sludge during aeration phase in sequencing batch reactor, Pol. J. Nat. Sci., 22 (2007) 246–255.
[55] Y. Bai, Q. Sun, D. Wen, X. Tang, Abundance of ammonia-oxidizing bacteria and archaea in industrial and domestic wastewater treatment systems, FEMS Microbiol. Ecol., 80 (2012) 323–330.
[56] Q. Ma, Y. Qu, W. Shen, Z. Zhang, J. Wang, Z. Liu, D. Li, H. Li, J. Zhou, Bacterial community compositions of coking wastewater treatment plants in steel industry revealed by Illumina high-throughput sequencing, Bioresour. Technol., 179 (2015) 436–443.